Acta Biomaterialia 197 (2025) 226–239

Contents lists available at ScienceDirect

Acta Biomaterialia

journal homepage: www.elsevier.com/locate/actbio

Full length article

Modeling and fabrication of MEW-3D tubular scaffolds with tendon mechanical behavior for tenocyte differentiation

Jorge Grasa [a,b], Ainhoa Urbiola [c,d], María Flandes-Iparraguirre [c,d], Leire Extramiana [d], Cristina Ederra [c,d], Carlos Ortiz-de-Solórzano [c,d], Rafael Llombart [d,e], Andrés Valentí [d,e], Enrique Baquero [f], Ángel Heras-Sádaba [a], Juan Pons-Villanueva [d,e], Begoña Calvo [a,b], Ana Pérez-Ruiz [c,d,g,*]

[a] Aragón Institute of Engineering Research (i3A), Universidad de Zaragoza, Spain
[b] Centro de Investigación Biomédica en Red en Bioingeniería, Biomateriales y Nanomedicina (CIBER-BBN), Spain
[c] Technological Innovation Division, Foundation for Applied Medical Research (FIMA), University of Navarra (UNAV), Spain
[d] Instituto de Investigación Sanitaria de Navarra (IdiSNA), Pamplona, Spain
[e] Orthopaedic Surgery and Traumatology Department, Clínica Universidad de Navarra, Pamplona, Spain
[f] Institute for Biodiversity and Environment BIOMA, University of Navarra, 31008 Pamplona, Spain
[g] Department of Biomedical Sciences, School of Health Sciences, Universidad CEU Cardenal Herrera, Valencia, Spain

ARTICLE INFO

Keywords:
Tendon
Scaffold engineering
MEW-3D
Tenocyte
Finite element method

ABSTRACT

Tendon injuries present substantial challenges in clinical settings, where traditional treatments often lead to suboptimal outcomes, including scar tissue formation, reduced strength, limited range of motion, and re-ruptures. These difficulties primarily arise from the complex hierarchical structure of tendons and their limited healing capacity. Tissue engineering offers promising solutions for tendon regeneration and muscle-to-bone reconnection, typically through the use of biodegradable scaffolds that mimic the extracellular matrix of tendons, thereby supporting cell growth and tissue formation. However, several obstacles must be addressed to develop tendon reconstruction strategies suitable for clinical application. In this study, we developed computational models to design and produce Melt Electrowriting (MEW)-3D tubular structures that replicate the mechanical properties of native mouse Achilles tendons, improving the guidance of tenocyte growth and differentiation. These models incorporated a new approach to consider the non-continuum nature of printed scaffolds formed by sets of fibers interacting with one another. Moreover, these structures facilitated cell confinement, expansion, and alignment, resulting in bundle-like formations with enhanced tensile properties. Importantly, tenocyte differentiation was achieved through a two-step cell culture protocol, which involved transitioning cells from high to low serum media. This approach effectively mitigated the phenotypic drift that often occurs with long-term cell cultures.

Statement of Significance

Tendon injuries are a common issue in healthcare, often leading to scar tissue, weaker tendons, limited mobility, and frequent re-injury. Tendon engineering aims to address these challenges by using biodegradable "scaffolds" that mimic the natural tendon environment, supporting cell growth and tissue repair. In this study, we developed computational models to design 3D tubular structures using a printing method called Melt Electrowriting (MEW). These structures replicate the mechanical properties of mouse Achilles tendons, guiding tendon cells to grow and differentiate effectively. By creating scaffolds from interwoven fibers, we closely replicated how natural tendon fibers interact, allowing cells to form strong, organized bundles. This approach may improve engineered tendon strength and durability, addressing key challenges in tendon reconstruction strategies.

* Corresponding author at: Department of Biomedical Sciences, School of Health Sciences, Universidad CEU Cardenal Herrera, Valencia, Spain.
E-mail address: ana.perezruiz@uchceu.es (A. Pérez-Ruiz).

https://doi.org/10.1016/j.actbio.2025.03.006
Received 30 October 2024; Received in revised form 1 March 2025; Accepted 4 March 2025
Available online 13 March 2025

1. Introduction

Tendon injuries are prevalent musculoskeletal clinical conditions, causing significant morbidity, pain, and long-term disabilities. Incidence rates vary based on demographics and lifestyle factors, with Achilles tendon (AT) injuries being particularly common, especially among athletes. Epidemiological studies report a notable worldwide increase in the incidence of AT rupture over recent decades [1–7].

Tendons play a vital role in the musculoskeletal system by connecting muscles to bones to transmit the force generated by muscle contractions. Primarily composed of collagen fibers organized in parallel bundles, tendons provide tension transmission and flexibility [8]. However, due to their reduced cellularity, low vascularity, and slow nutrient supply, tendons exhibit delayed and ineffective natural healing processes after injury, often resulting in scar tissue formation, causing permanent reductions in flexibility and tension capacities. Various surgical techniques exist to reconstruct tendon ruptures, using tendon transfers, tenodesis or biological and synthetic grafts [9]. However, these methods have limitations, such as morbidity, disease transmission, or immune responses in human recipients [10,11]. Additionally, repaired tendons often exhibit biomechanical properties inferior to native ones, increasing susceptibility to re-rupture [12]. This situation is particularly challenging in the AT, as it is the largest and strongest tendon in the human body, capable of withstanding forces that exceed 12 times the body weight during basic activities [13]. The absence of optimal solutions poses a significant challenge for orthopaedic surgeons, emphasizing the need for a healing bridge that mimics native tendon properties for effective repair or reconstruction.

Tendon engineering aims to develop artificial tissues for clinical purposes [14,15]. However, significant challenges remain, such as guiding cell alignment, migration, proliferation, and differentiation within printed constructs to accurately replicate the intricate structure of tendons [15,16], including their heterogeneous and anisotropic extracellular matrix (ECM). This is crucial for ensuring adequate loading capacity [17] and for guaranteeing the efficacy and longevity of the engineered tendons [18]. Various technologies aim to fabricate 3D scaffolds that replicate the anatomical features and mechanical properties of native tendons. Among these, electrospinning is the most widely used method. It allows for the incorporation of aligned and/or random fibers, which favor tendon structural organization, efficient force transmission and stress distribution or help emulate the tendon-bone transition [19–21]. Electrospinning can also be used for the creation of sinusoidal-like morphologies in the nanofibers [22–25], which is important because variations in the crimped pattern of submicron-sized collagen fibrils affect the mechanical properties of tendons. Additionally, it can integrate grooved structures to guide cell differentiation [26] or be used to prepare spun fibrous scaffolds through braiding or weaving aligned nanofiber yarns [27]. However, while these advancements allow for precise control over pore size and approximate the nonlinear tensile strain–stress behavior of tendons, they often prioritize mechanical properties or cell-to-tendon transformation. For example, crimped nanofibrous scaffolds increase mechanical performance but limit cellular infiltration and alter the behavior of seeded cells by reducing scaffold porosity [24]. Furthermore, the development of a rich ECM in cell-assembled tendon equivalents necessitates prolonged *in vitro* cell cultures. These extended culture periods are often associated with cellular phenotypic drift [28,29], which compromises the quality and functionality of the engineered tissue. Moreover, since scaffolds serve as temporary structures that support tissue growth, their properties must mimic those of natural tendon tissue to facilitate proper regeneration. Scaffold design presents another potentially challenge, particularly when applying the finite element method (FEM) to Melt electrowritting (MEW) scaffolds due to their intrincate nature. MEW structures are typically composed of fine, microscale fibers arranged in complex and often irregular patterns. Accurately capturing these features in FEM simulations requires a high level of mesh resolution, which in turn increases both computational demands and complexity [30]. Addressing these challenges is critical for the advancement of tissue-engineered tendon replacements and their successful clinical application.

Here, we have employed MEW additive manufacturing technology to create highly defined 3D scaffolds with controllable architecture. These scaffolds are designed as confinement structures to support cell-to-tendon conversion, intentionally excluding the influence of scaffold pore size and geometry on human tenocyte properties. At the same time, they preserve the tensile strength of murine AT and replicate its characteristic tubular, bundled structure. To achieve this, we have developed a new constitutive model within a continuum framework using FEM to predict the mechanical behavior of tubular scaffolds. This numerical technique allowed us to select specific printing parameters to closely mimic the native AT structure of mice. These tubular constructs sustain human tenocyte expansion, alignment, and differentiation, and provide the compliance and tensile strength of the original tendons. The implementation of a two-step cell culture protocol, with static force guides, permits the long-term culture of human tenocytes to create an ECM tendon-like structure with an enhanced mechanical behavior. The scalable manufacturing process of the 3D structures can be easily adapted for producing scaffolds in various sizes and geometries, from small-scale research prototypes to large-scale clinical implants. These insights have significant potential applications in tendon regenerative medicine.

2. Materials and methods

2.1. Melt electrowriting (MEW)

Fibrous tubular scaffolds were manufactured via MEW, using a custom-built MEW device (Queensland University of Technology) with medical grade poly-ε-caprolactone (mPCL) pellets (Purasorb PC12, Corbion). The mPCL jet was left to stabilize until its deposition was homogenous (no coiling or pulsing). The fiber was collected onto a rotating mandrel of 1 mm in diameter, with a 7 mm printing distance form collector. Tube manufacturing was achieved by moving the nozzle back and forth in the longitudinal direction. All tubes were manufactured with a voltage of 8.9 ± 0.3 kV, and consisted of 300 layers, understanding one layer as the full movement of the nozzle.

SEM Microscope. A Scanning Electron Microscope (SEM) was utilized to obtain high-resolution and high-contrast images of the MEW-3D constructs. To this end, scaffolds were mounted on aluminum SEM stubs and coated in an Argon atmosphere with 16 nm gold in a sputter-coater device (Emitech Ltd., Strovolos, Chipre, model K550). SEM observations were made with a FE-SEM Zeiss model Sigma 300 VP (Zeiss, Oberkochen, Germany).

2.2. Mechanical analysis

The biomechanical behavior of the MEW-3D tubular structures and the native mouse AT were studied using an electromechanical Instron Microtester 5248 testing setup (Illinois Tool Works Inc., Glenview, IL, USA), equipped with a 5 N load cell with minimal resolution of 0.001 N. The tendons were tested immediately after sacrificing the animals, which were carefully isolated. MEW-3D structures and tendons were subjected to a displacement rate of 3 mm/min until failure, $N = 5$. Force and displacement were acquired at 10 Hz and recorded in a data file for further processing.

2.3. Culture of human tenocytes

Tenocytes were isolated from human tendon biopsies, obtained during surgical procedures from discarded hamstring tendon tissue for anterior cruciate ligament reconstruction after written informed consent in the Clínica Universidad de Navarra (CEI 2019.116), or from cadavers (CEI 2020.22), following mechanical and enzymatic digestion with collagenase II/Dispase I for 16 h at 37 °C. For 2D cell cultures, 20,000 tenocytes were cultured in 12-well dishes previously treated with Matrigel (*Becton&Dickinson*). Cells were maintained in growth medium (GM), consisting of 20% foetal bovine serum (FBS), 1% penicillin-streptomycin, and $2x10^{-3}$ M L-glutamine in Dulbecco's Modified Eagle Medium (DMEM), at 37 °C and 5% CO_2 for 7 days. Subsequently, some cells continued in GM, while others underwent a switch to differentiation media (DM) composed of 2% FBS in DMEM. Cells were maintained under these conditions for a 16-day period.

For 3D cultures, cells maintained in GM at low cell density were collected, embedded in Matrigel, and casted into the mPCL-printed tubular structures. These 3D structures were previously treated with O_2Ar plasma (Diener electronic, Plasma-surface-technology, Ebhausen, Germany) for 2 min to reduce the structure hydrophobicity, washed in ethanol, air-dried and exposed to ultraviolet light. The cell composites were incubated at 37 °C for 30 min in 6-well dishes, after which GM was added to cover the structure. After 11 days, cell composites were subjected to tension from both ends using microsurgical clamps (*S&T*, 70008) and maintained in culture for an 18-day period. Then, GM was replaced by DM for 34 days. GM and DM were changed every three days.

Some cell-free constructs embedded in Matrigel were pre-treated and treated as the cell-filled Matrigel composites for 9 weeks, and were used as controls.

2.4. Morphological and phenotypical characterization of 2D and 3D tenocytes

Immunofluorescence. Cell composites were washed in PBS and fixed in 4% paraformaldehyde (PAF) for 10 min at room temperature. After several PBS-washes, constructs were secured in 3% gelatine and frozen in OCT. Constructs were longitudinally cryosectioned in 50–100 μm sections, collected on silane:acetone (1/10) treated-slides, and kept at −80 °C until use. 2D cell cultures were fixed in 4% PAF and stored at 4 °C. Both 2D cells and 3D sections were permeabilized with 0.5% Triton-X100/PBS for 5 min and incubated in blocking solution (BS; 20% goat serum/PBS) for 30 min. Then, collagen I (5 μg/ml; BioRad), tenomodulin (10 μg/ml; Santa Cruz), decorin (10 μg/ml; Santa Cruz), scleraxis (10 μg/ml; Santa Cruz) and β-tubulin (5 μg/ml; Cell Signaling) antibodies were diluted in BS, added to the samples and incubated at 4 °C overnight. Primary antibodies were visualized with fluorochrome-conjugated secondary antibodies (Molecular Probes) before mounting in 0.1% glycerol/PBS medium. Nuclei were visualized by pre-treating the living or fixed cells with 1X SPY live cell fluorogenic DNA labeling probe (Spirochrome), following manufacture's instructions. Stained cells and 3D sections were kept in PBS at 4 °C in dark until their use.

Image acquisition and processing. Tile and z-stack scans from living cell composites, fixed 2D cells or fixed 3D sections were imaged combining 2-photon and confocal mode. A Zeiss LSM 880 microscope (Carl Zeiss, Jena, Germany), equipped with a 2-photon femtosecond pulsed laser (MaiTai DeepSee, Spectra-Physics, Newport USA), was tuned to a central wavelength of 790 nm using a 25×/0.8 objective (LD LCI Plan-Apochromat 25×/0.8, Carl Zeiss) in non-descanned mode after spectral separation and emission filtering using 465-to 515-nm BP filters. Confocal emission between 650–750 nm and 560–660 nm was obtained by using the 633 nm and 543 nm lasers, respectively.

Digital images were processed using Zen lite 3.0 and ImageJ software. When needed, images were composed and edited, and modifications were applied to the whole images using Photoshop CS6 (Adobe, 2015.1 version).

Cell alignment and nuclei roundness analyses. Image stacks from 2D and 3D samples were used for quantifying cell orientation and elongation. Eight different planes were analyzed per cell composite, with an average mean of 292 cells per plane. One or two planes in two different regions were analyzed in tenocytes grown in 2D, with an average mean of 416 cells per plane. Nucleus orientation and roundness were measured using a built-in function of ImageJ software.

Quantitative real time-PCR (qPCR) analysis. Total RNA was extracted directly from culture dishes with TRIzol (Sigma) following the manufacturer's instructions. RNA content and purity were determined using a Nanodrop (Qiagen). Retro–transcription was performed using the Prime Script RT Reagent (Takara) with up to 1 μg of RNA for each sample.

qPCR was performed with 10 *ng* of cDNA with the Applied Biosystems™ PowerUp™ SYBR™ Green Master Mix in a QuantStudio 5 real–time PCR thermocycler by using specific primers (Forward: $5' - 3'$; Reverse: $5' - 3'$) for collagen type I (*COL1A1*: AGAAGAACTGGTACATCA; CATACTCGAACTGGAATC), collagen type III (*COL3A1*: ATCTTGGTCAGTCCTATG; TATTATGTCATCGCAGAGA), scleraxis (*SCX*: CACCCAGCCCAAACAGAT; CACCTCCTAACTGCGAATC), tenomodulin (*TNMD*: ACAAGCAAGTGAGGAAGAA; GACGGCAGTAAATACAACAAT), and tenascin (*TNC*: CCTTGCTGTAGAGGTCGTCA; CCAACCTCAGACACGGCTA). Glyceraldehyde–3–phosphate dehydrogenase (*GAPDH*: TTTAACTCTGGTAAAGTGGATAT; GGTGGAATCATATTGGAACA) was selected as endogenous control. Primer specificity was confirmed by melting curve analysis. All samples were measured in triplicate in at least three independent experiments. Relative mRNA levels were calculated by the $2 - \Delta\Delta Ct$ method.

Cell viability. 2D cell cultures were stained with the cell death detection antibody in the Zombie–Green Fixable Viability Kit (423111, BioLegend) following the manufacturer's protocol. Samples were acquired with a CytoFlex flow cytometer (Beckman Coulter) and data analyses were performed using FlowJo software.

2.5. Constitutive material modeling

A strain energy density function (SEF) is a mathematical formulation used in continuum mechanics to describe the energy stored in a material due to deformation. To simulate the properties of mPCL scaffolds operating within the elastic regime, a suitable SEF should account for both nearly incompressible [31] and non-linear elastic behavior [32]. When this material is used to print complex 3D structures, applying the continuum mechanics hypothesis presents a significant challenge. To address this, we propose an approach that involves modeling the entire scaffold volume using a SEF as follows:

$$\Psi = \phi\Psi' \qquad \phi = \frac{V_s}{V_T} \tag{1}$$

where ϕ represents the volume fraction of the material, with $(1 - \phi)$ corresponding to the scaffold's porosity, defined as the gaps within the total volume where no material is present. Therefore, Ψ' can be defined as:

$$\Psi' = \Psi_{vol}(J) + \bar{\Psi}(\bar{I}_1, \bar{I}_4, \bar{I}_6, \bar{I}_8) = \frac{\kappa}{2}(J-1)^2 + \bar{\Psi}_1 + \bar{\Psi}_4 + \bar{\Psi}_6 + \bar{\Psi}_8 \tag{2}$$

In this expression, the volumetric part of the SEF, Ψ_{vol}, depends on the PCL bulk modulus (κ) and the determinant of the deformation gradient (J), the jacobian. The volume-preserving part has been defined as a function of the first modified invariant of the right Cauchy–Green deformation tensor ($\bar{I}_1$) and three pseudo-invariants ($\bar{I}_4, \bar{I}_6, \bar{I}_8$), associated with the printed preferential directions. The pseudoinvariants $\bar{I}_4$ and $\bar{I}_6$ are defined as:

$$\bar{I}_4 = \mathbf{a}_0 \cdot (\bar{\mathbf{C}}\mathbf{a}_0), \qquad \bar{I}_6 = \mathbf{b}_0 \cdot (\bar{\mathbf{C}}\mathbf{b}_0) \tag{3}$$

where $\mathbf{a}_0$ and $\mathbf{b}_0$ are the initial orientations of the PCL fibers. To account for the interaction between these fibers, we propose using an additional

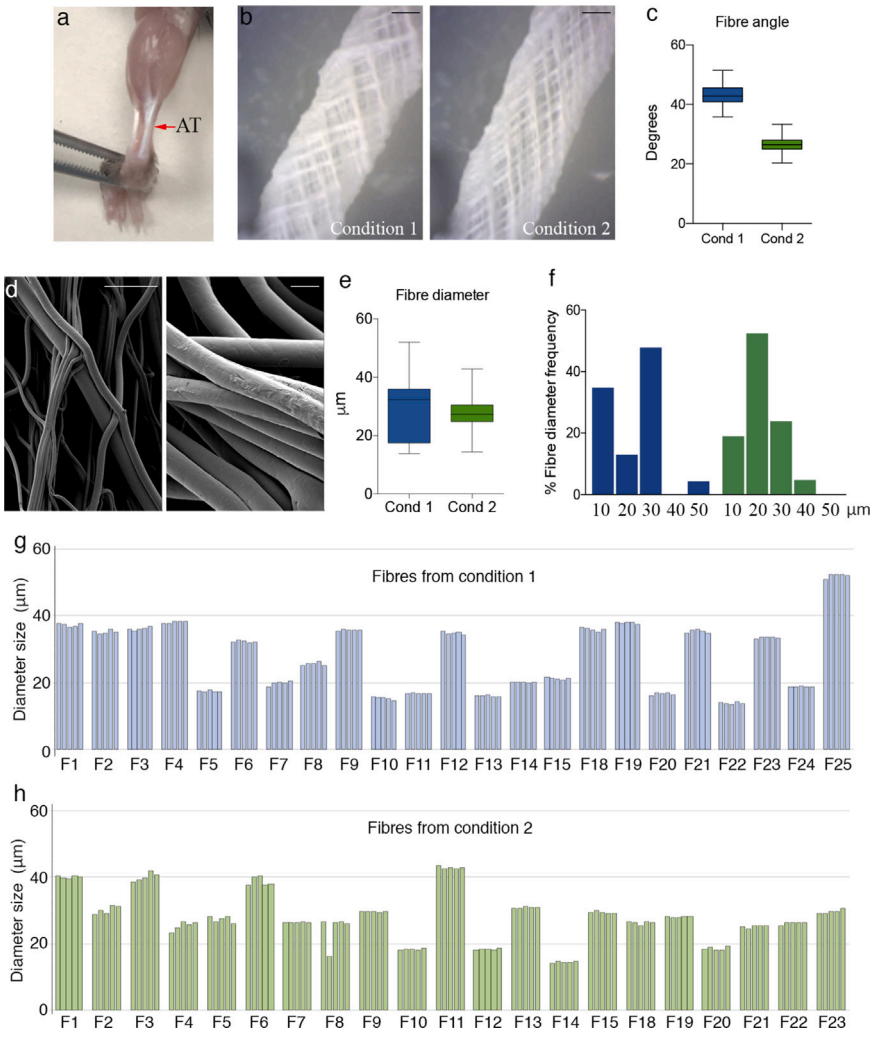

Fig. 1. Achilles tendon (AT) of an adult wild type mouse (a). Representative images of printed scaffolds (b; scale bar: 0.5 mm) and quantification of fiber angle (c). Representative images of the tubular scaffolds taken by SEM microscopy (d; scale bars: 200 µm (left) and 20 µm (right)). Average (e) and frequency distribution (f) of fiber diameters. Diameters from fibers from condition 1 (g) and condition 2 (h) were measured at five different positions. Data was collected from 5 independent replicates of each condition (n=5). F, Fiber; Cond, condition.

pseudoinvariant to capture the angle change ($\Delta\varphi$) between the two fiber directions [33]:

$$\bar{I}_8 = \Delta\varphi = \varphi - \varphi_0 \approx \left(\bar{I}_4\bar{I}_6\right)^{-\frac{1}{2}} \mathbf{a}_0 \cdot (\mathbf{C}\mathbf{b}_0) - \mathbf{a}_0 \cdot \mathbf{b}_0 \tag{4}$$

The SEF functions have been chosen in the form of the well-known fiber contribution commonly used in the biomaterials field [34]. The function $\bar{\Psi}_1$ represents the isotropic contribution of the scaffold material in regions where the fibers have fused together.

$$\bar{\Psi}_1 = \frac{1}{2}c_1\left(\bar{I}_1 - 3\right)^2 \tag{5}$$

Since the fibers were deposited in two distinct directions during printing, corresponding to the forward and backward movement of the nozzle, $\bar{\Psi}_4$ and $\bar{\Psi}_6$ represent the elastic energy of the anisotropy induced by these directions:

$$\bar{\Psi}_4 = \frac{k_1}{2k_2}\left(e^{k_2\left(\bar{I}_4-1\right)^2} - 1\right), \qquad \bar{\Psi}_6 = \frac{k_1}{2k_2}\left(e^{k_2\left(\bar{I}_6-1\right)^2} - 1\right) \tag{6}$$

The elastic energy associated with the **fiber** angle change is expressed as:

$$\bar{\Psi}_8 = k_3\left(\bar{I}_8\right)^2 \tag{7}$$

The model parameters c_1, k_1, k_2, and k_3 in the function will be calibrated based on experimental results.

2.6. Statistical analysis

All statistical analyses were performed using SPSS 26.0 (SPSS, Inc., Armonk, NY, USA). The Shapiro–Wilk test was used to assess the normality of the data distribution. When the data were non-normally distributed, variables were analyzed using the Kruskal–Wallis test, followed by Mann–Whitney U tests for pairwise comparisons. When the data were normally distributed, Levene's test was performed to assess the equality of variances. If the variances were equal, t-tests were performed for pairwise comparisons. If the variances were unequal, Welch's test was used instead. For comparisons involving more than two groups, one-way ANOVA was performed, followed by post-hoc analyses using Bonferroni and Tukey's HSD tests. All experiments were performed with at least three independent biological replicates per condition. Data are expressed as means ± standard error of the mean (sem). A p-value of $p < 0.05$ was considered statistically significant.

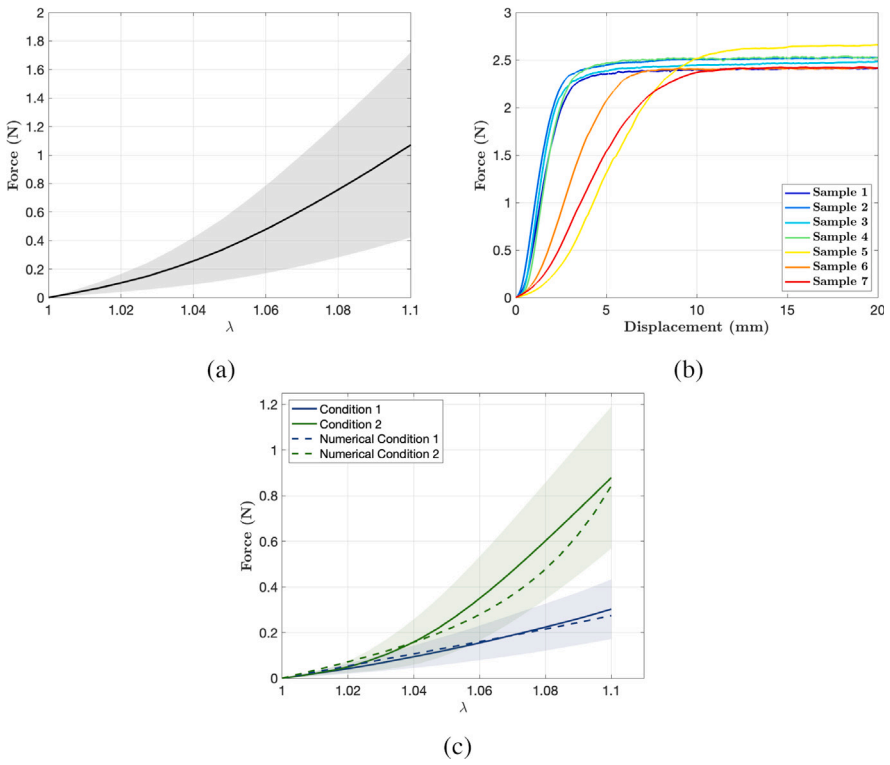

Fig. 2. Experimental characterization: Force vs stretch of mouse Achilles tendon samples (a), force vs displacement of seven MEW-3D skeletons with the fibers oriented at 26.6° (b), mean and standard deviation of the force vs stretch relationship considering both printing conditions together with numerical model predictions (c).

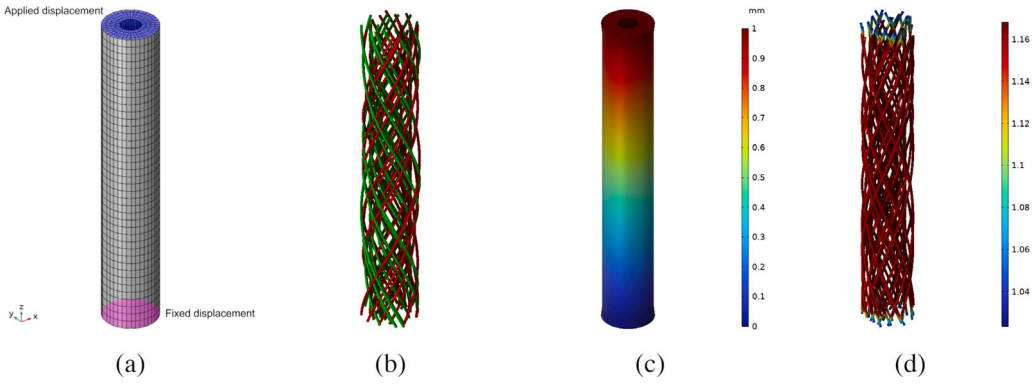

Fig. 3. FE model and results: FE mesh (a), representation of the two family of fibers oriented at 26.6° (b), displacement field along the z direction (c) and representation of the stretch along the fibers (d).

3. Results

3.1. Design and fabrication of MEW-3D tubular structures with tendon mechanical behavior

We designed and fabricated tendon-mechanical biomimetic 3D tubular skeletons formed of mPCL fibers to replicate healthy native tendons, characterized by their fibro-elasticity and resistance to mechanical tension. Fabrication was designed based on the anatomical features of the AT isolated from adult mice (Fig. 1a), which presented a diameter of 0.67 ± 0.02 mm and a length, from the calcaneus to the proximal insertion in the calf muscles, of 6.41 ± 0.33 mm.

The structures were fabricated with a MEW-printing system by simply tuning the rotational speed of the motor and collecting the mPCL fibers on a 1 mm diameter cylindrical mandrel in continuous rotation. By changing the orientation of the fibers with respect to the horizontal axis, considering both the translation velocity and the rotating speed of the mandrel, we defined two different sets of printing conditions. Condition 1, involved a translation speed of 285 mm/min and a rotation speed of 400°/min, and its outcome was fibers arranged at $43.2 \pm 3.5°$ (Fig. 1b–c). Condition 2, consisting of 500 mm/min and 350°/min, resulted in a fiber orientation of $26.6 \pm 2.6°$ (Fig. 1b–c).

To determine the spatial distribution and microscale structure of the MEW constructs, samples were subjected to SEM. At high magnification (Fig. 1d), the average diameter size of individual fibers was 27.87 ± 0.9 μm and 28.16 ± 0.71 μm for conditions 1 and 2 (Fig. 1e), respectively. Independently of specific printing parameters, individual fibers size ranged from 10 to 50 μm in diameter (Fig. 1f). Fibers with 30 μm were the most frequent size for condition 1, while condition 2 showed a preference for fibers with a 20 μm of size (Fig. 1f). Furthermore, measurements taken at various lengths from the same mPCL fiber plane were similar (Fig. 1g–h), indicating homogenous printing along the longitudinal direction. Importantly, by using a cylindrical mandrel of 1 mm of diameter to collect the printed fibers, the final internal size of the 3D structures was 0.65 ± 0.4 mm, fitting the dimensions of the

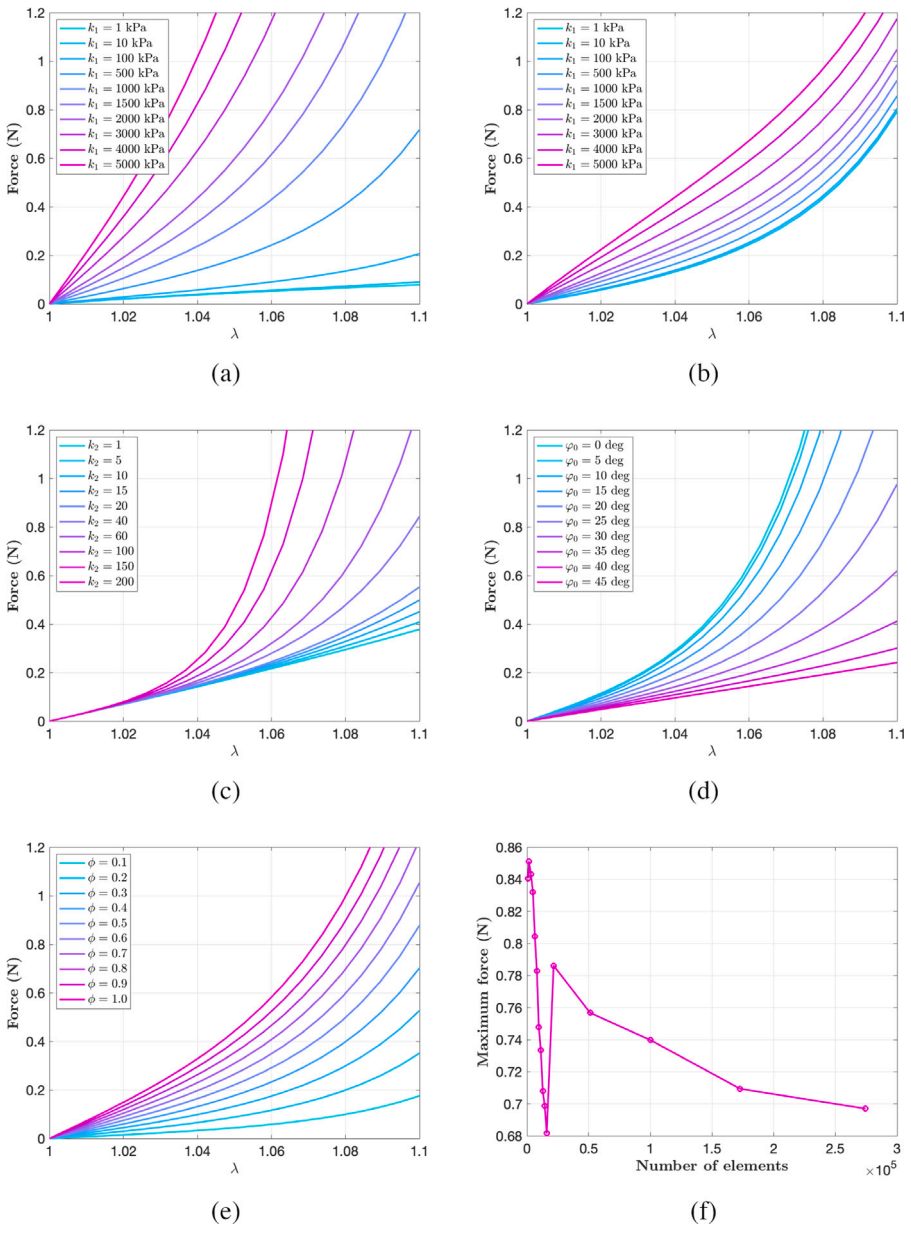

Fig. 4. Sensitivity analysis of different parameters in the model: effect of constitutive parameters k_1 (a), k_2 (b), and k_3 (c), initial fiber angle orientation (d), scaffold volume fraction (e) on the force vs. stretch relationship, and mesh size (f) on the maximum force.

AT of adult mice. This dimension, together with the external diameter, allowed us to obtain an approximate volume fraction of the material by knowing the density of the bulk mPCL (1.145 g/cm^3) and weighing the samples. The volume fractions for samples under conditions 1 and 2 were 0.51 ± 0.23 and 0.48 ± 0.37, respectively.

We next analyzed the uniaxial tensile behavior of the AT samples isolated from mice. The curve in Fig. 2a represents the relationship between force and the stretch ratio (λ), showing the mean response of the tendon samples under tension, with the standard deviation depicted as the filled region.

Force–displacement curves for the samples with fibers arranged at $26.6 \pm 2.6°$ are shown in Fig. 2b. Analyzing these curves, it is observed that there is an initial region where a non-linear relationship between the applied force and displacement is obtained, followed by a drastic change in slope as the scaffold enters the plastic deformation zone. Fig. 2c shows the mean and standard deviation of the experimental and numerical predictions force vs. stretch relationship (solid line) for the two conditions. As observed, by varying the printing angle, the optimal value for reproducing the J-shaped stress–strain curves of the tendon can be determined.

3.2. Computational modeling

The finite element (FE) model (Fig. 3a) is defined as a tube with a length of 10 mm, an inner diameter of 0.65 mm, and an outer diameter of 1.53 mm. The model reproduces the tensile test carried out experimentally by embedding one of the ends and applying a displacement of 1 mm in the longitudinal direction until an elongation of $\lambda = 1.1$ is achieved.

To define the anisotropy induced by the mPCL fiber structure, two families of fibers were created in the software according to the fabrication conditions. In Fig. 3b the discretized distribution of these orientations are represented for condition 2. The continuous model implemented in Comsol Multiphysics allows for the visualization of mechanical variables, such as displacements in the continuum geometry

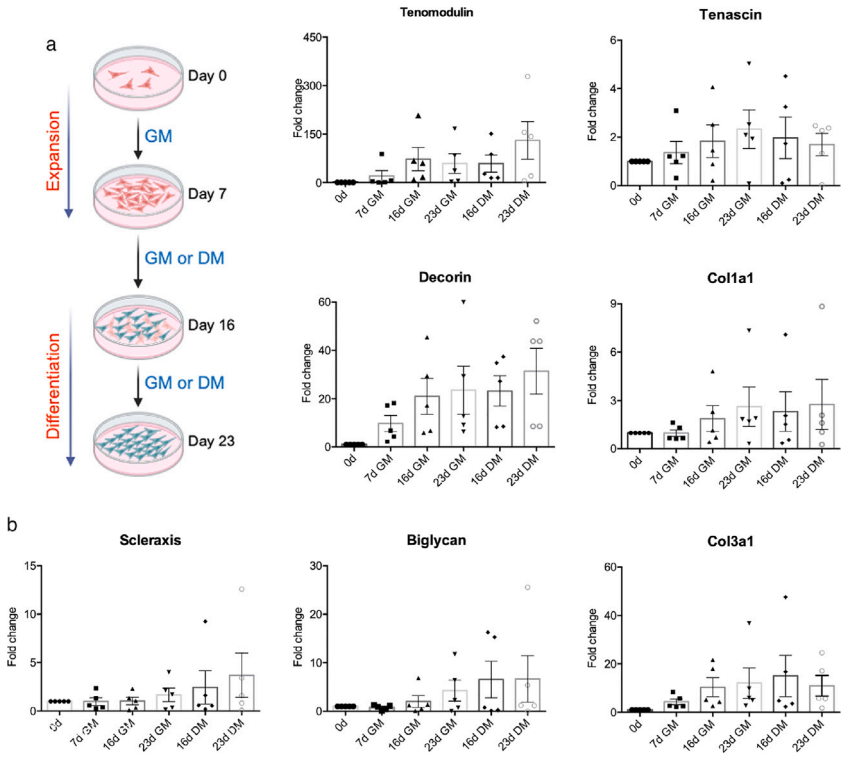

Fig. 5. Experimental schematic outlining the cell culture protocols (a). Graphs in b show mRNA expression levels of genes associated with tenocyte differentiation in differentiated cells, relative to GAPDH expression levels. Data is expressed as mean±sem from five independent experiments carried out with cells obtained from different donors (n=5), where expression levels were related to those found at day 0, which were considered as 1.

(Fig. 3c), or the deformation in the deformed configuration of the fibers (Fig. 3d).

Before determining the model parameters that best fit the hyperelastic behavior of the available experimental data, a sensitivity analysis was conducted to understand their effect on the reaction force in the model during stretching. Figs. 4a, 4b, and 4c illustrate the sensitivity to the mechanical parameters k_1, k_2, and k_3, showing the effect of fiber stiffening and their interactions. Fig. 4d depicts the effect of fiber orientation, with $\varphi_0 = 0$ representing the extreme angle when the fibers are aligned parallel to the longitudinal direction of the scaffold. As observed, as this angle increases, the force required to stretch the scaffold decreases. Fig. 4e shows that lower values of porosity correspond to a stiffer structure, indicating the effect of material volume fraction. Finally, Fig. 4f illustrates the effect of the number of elements in the finite element mesh on the force at a stretch level of $\lambda = 1.1$. As observed, above approximately 50,000 elements, the solution varies by less than 2%.

In order to find the constitutive parameters that allow the model to predict the experimental tests of the scaffolds under the two fabrication conditions, a series of Monte Carlo simulations were conducted. In these simulations, the parameter range of variation was gradually decreased until the root mean square error (RMSE) was less than 0.1 N. The parameters found that provided an RMSE of 0.012 N for condition 1 and 0.066 N for condition 2 were: $c_1 = 100$ kPa, $k_1 = 600$ kPa, $k_2 = 40$, $k_3 = 400$ kPa. A value of $\kappa = 1$ GPa was assumed for the bulk modulus of the mPCL taking and elastic compressive modulus of $E = 300$ MPa [35] and a Poisson's ratio of $\nu = 0.45$ [36], being $\kappa = E/(3(1-2\nu))$. Fig. 2c represents the numerical force vs. stretch predictions of the model compared with the mean and standard deviation outcomes of the experiments.

3.3. Scaffold colonization

A high-to-low serum transition enhances tenocyte differentiation

We next proceeded to select a cell culture protocol aimed at facilitating the tenogenic differentiation of undifferentiated cells into tendons. We selected human tenocytes from various sources due to their inherent potential to differentiate into tendon tissue. Instead of using biochemical growth factors or transforming growth factors to induce tenocyte differentiation [37], we employed an alternative strategy. After seeding the cells in Matrigel-coated 6-well dishes, they underwent a 7-day expansion phase in mitogen-rich medium (GM), followed by a 16-day differentiation period in mitogen-poor medium (DM) containing 2% of serum, or they were maintained in GM throughout the experiment (Fig. 5a). Tenocytes transitioned from GM to DM showed a tendency to increase the expression levels of the tenogenic genes scleraxis, tenomodulin, decorin and biglycan over time, compared to those continuously maintained in GM (Fig. 5b). However, the expression of tenascin and collagen mRNA was not affected by the two-step cell protocol (Fig. 5b). The absence of statistically significant differences among tenocytes cultured under different protocols may be attributed to the diminished tenogenic potential of older cells [38,39] rather than a decrease in cell viability. This conclusion is supported by distinct variations in gene expression levels observed between tenocytes isolated from young patients undergoing surgery (young samples) and those obtained from cadavers (old samples) (Figure S1a). Importantly, no signs of cell death were observed in old tenocytes across both experimental conditions (Figure S1b).

To further corroborate the differentiation phenotype, immunostaining was performed in young tenocytes. This technique confirmed the increased accumulation of tenomodulin and decorin proteins in the cytoplasm of the cells as they underwent differentiation (Fig. 6a). Notably, this accumulation appeared more pronounced in cells transitioning from high to low serum media (Fig. 6a). Correspondingly, the nuclear Scx signal was lost in differentiated cells, though some cells in GM retained positive nuclear signals (Fig. 6b, arrows). Collagen I accumulated in the cytoplasm of differentiated tenocytes, with their cytoskeleton aligned into defined, larger fiber-like structures (Fig. 6b–c). However, the presence of collagen I in the extracellular space was

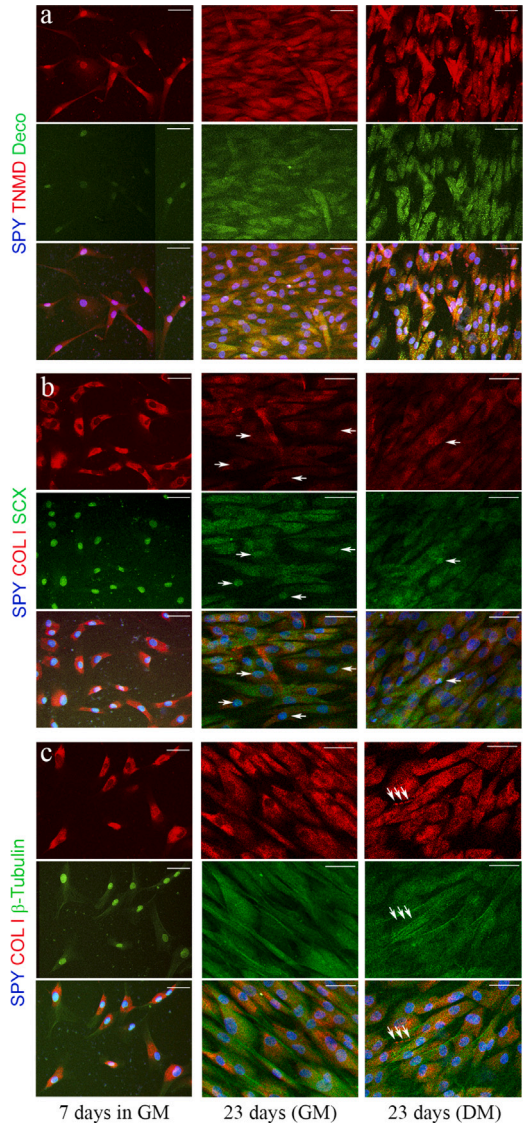

Fig. 6. Representative images of tenocytes co-immunostained for tenomodulin/decorin (a), collagen I/scleraxis (b), and collagen I/β-tubulin (c) under growth (GM) and differentiation (DM) culture conditions over time. SPY identified all nuclei. Scale bar 20 μm. All cell images were taken at the same exposure time.

more frequent in cells cultured in DM (Figure S2c, arrowheads), with some spots forming fibril-like structures (Fig. 6c, arrows; Figure S2, arrows), compared to cells continuously maintained in GM, suggesting a more advanced stage of collagen maturation. Taken together, these findings reinforce the idea that cells transitioning from high to low serum content, without the addition of tenogenic promotion factors, exhibit a more advanced differentiation phenotype.

Tubular MEW-3D scaffolds allow for tenocyte growth and differentiation

To expand and differentiate human tenocytes within the tubular scaffolds, we selected those composed of fibers arranged at a 26.6° angle, as they more accurately mimic the mechanical behavior of native mouse tendons (Fig. 2a), and adopted a systematic cell culture approach based on our earlier findings (Fig. 7a). The cells were embedded in Matrigel, introduced into the tubular constructs (referred to as cell composites), and maintained in culture for a period of 9 weeks. Following an initial 10-day period in GM, static mechanical stimulation was applied both to guide the cells, as tendons undergo physiological mechanical stretching during their functioning, and to enhance cell proliferation [40]. After a 45-day period in GM to ensure thorough cell colonization of the structure, the cell composites underwent an 18-day phase in DM to enhance tenocyte differentiation. We extended cell expansion period due to slower proliferation of cells in 3D compared to 2D, likely because 2D cultures allow better access to essential components in the medium [40,41] and offer increased mechanical stiffness, promoting cell growth [42,43]. Throughout this 9-week timeline, the progression of cell composites was non-invasively monitored using optical (Fig. 7b) and multiphoton imaging (Fig. 7c–i). The inherent autofluorescence of both fabricated mPCL scaffolds (Fig. 7c) and cells (Fig. 7d–i) was harnessed to capture and analyze the tenogenic progression of the cells and their interaction with the 3D structures.

By week 1, we observed that tenocyte growth was restricted to the scaffolds (Fig. 7d; Figure S3a), with some cells interacting with the mPCL fibers within the constructs (Fig. 7e). Z-stack imaging revealed a progressive increase in cell density over time (Fig. 7f–i), demonstrating that confining cells within the 3D structures promotes homogeneous cell growth at any depth (Figure S3b–e). Following the stretching of the constructs, there appears to be an enhancement in the cytoplasm-to-nuclei (Fig. 7f–g; Figure S3b–c), a phenomenon that intensified upon transitioning from GM to low-mitogen media (Fig. 7h–i; Figure S3d–e). This was evidenced as an increase of the number of tenocytes aligned along the longitudinal axis of the stretched construct skeletons (Fig. 7g; Figure S3e), which trend persisted throughout the culture period, as evidenced in later time points (Fig. 7h–i; Figure S3d–e).

By week 9, nuclei within some living cell composites were visualized, demonstrating the colonization of the constructs by tenocytes (Fig. 8a) and the formation of cell bundle-like structures at various depths within the cell composites (Fig. 8b–d). To assess the alignment of tenocytes, we analyzed the position of their nuclei within the longitudinal axis of the 3D structure, distinguishing 5 relative positioning degrees (Fig. 8e). Tenocytes in composites exhibited a notable preference to align along one main direction, in contrast to tenocytes grown in 2D cultures (Fig. 8f), which displayed a more random alignment. Furthermore, the preferential positioning of the cells within the 3D structures was consistently maintained at different depth levels, as evidenced by analyses performed at various z-stacks (Figure S4). Additionally, the quantitative analysis of nucleus elongation demonstrated an increasing predisposition of cells within the composites to enlarge their nuclei (Fig. 8g), compared to cells within 2D cultures. Finally, we assessed the stress–strain curves of living cell composites by week 9, finding that their tensile properties increased in comparison to cell-free Matrigel-embedded constructs (Fig. 8h), which were subjected to the same protocol paute than the cell-filled Matrigel composites. This outcome suggested the production of ECM components by human tenocytes within the 3D structures, corroborating their differentiated phenotype.

Together, these findings showed that the MEW tubular constructs influence tenocyte behavior, growth, and differentiation, offering valuable insights into potential applications for tissue engineering.

Cell composites express tenogenic differentiation makers

To confirm the tenogenic differentiated pattern of cell composites, expression of specific cell markers was analyzed by immunostaining at week 9, after scaffold cryosectioning.

The cell composites expressed collagen type I both in the vicinity of the mPCL fibers (Figure S5a–c) and in bundle tendon-like structures (Fig. 9a; Figure S5d–f), which co-expressed tenomodulin (Fig. 9b; Figure S6a–d). Tenomodulin expression was more evident in aligned cells (Fig. 9b; Figure S6a–d) than in non-aligned ones, where scleraxis was mostly related to the nuclei of the tenocytes (Fig. 9c; Figure S6e–h). Additionally, collagen type I and decorin co-immunostaining (Fig. 9d) confirmed ECM production by the cell composites, while β-tubulin showed the cytoskeleton of the cells, which in addition to highlight their positioning suggested the connection between the cells (Fig. 9e–f; Figure S7a–i) and between the cells and the mPCL fibers (Fig. 9g; Figure S7j–l). These findings suggest that the mechanical static stimulation given to the cell composites is transmitted to the entire construct,

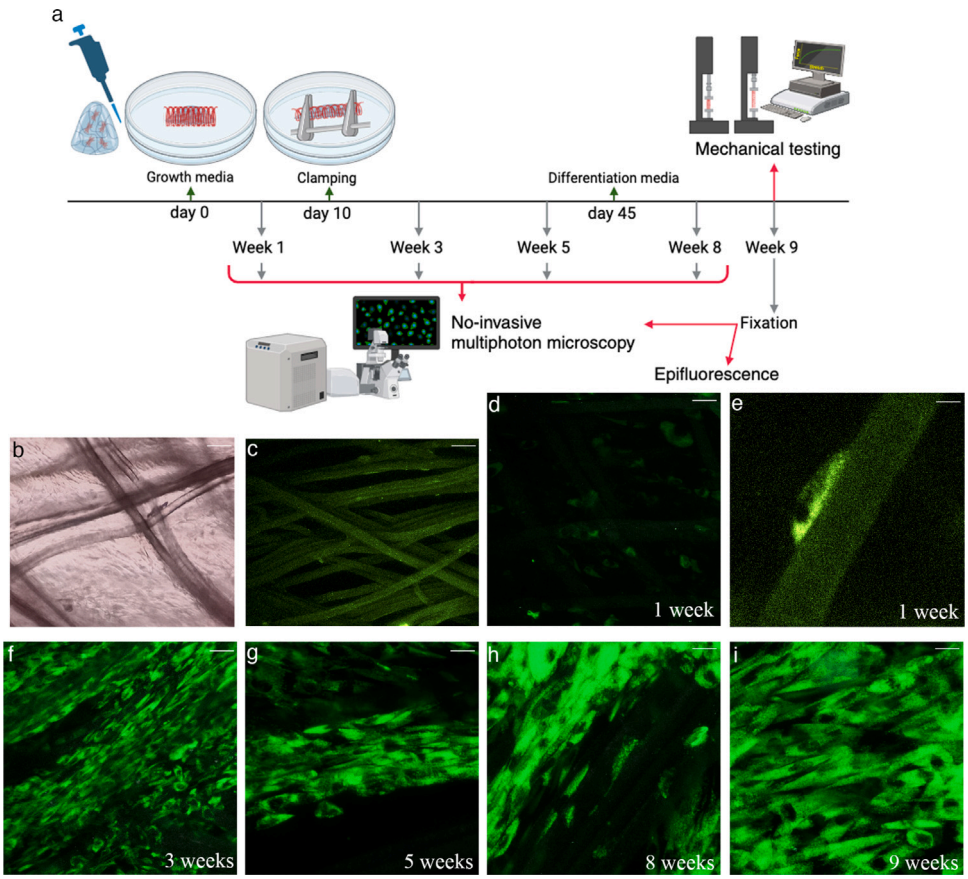

Fig. 7. Schematic picture outlining the colonization of the MEW-3D structures and the analyses followed for their characterization (a). Representative optical image of cultured tenocytes in the 3D tubular structures (b). Autofluorescence of the PCL fibers (c) and tenocytes (d–i) overtime, captured by non-invasive microscope. All cell images were taken at the same exposure time. A total of four cell composites were analyzed at each time point (n=4). Scale bar: 20 μm.

since the cytoskeleton is a 3D network that can transmit biomechanical stimuli between the extracellular and intracellular environments by connecting the nucleus to the ECM, regulating many cellular functions, including cellular differentiation.

4. Discussion

There has been a growing interest to fabricate artificial tendons over recent decades [44,45]. However, despite extensive efforts to optimize scaffold design by incorporating physical and biochemical stimuli to promote tendon regeneration [46–48], their clinical translation remains challenging. One major obstacle is the mechanical mismatch between the artificial tendon and the recipient tissue, which can lead to local inflammation, reduced cell viability, and limited cellular stimulation, thereby impeding the overall healing process [49,50]. Another challenge lies in promoting the appropriate cellular responses within the scaffold to ensure adequate cell alignment and differentiation with a robust ECM structure [51], crucial for optimizing tendon repair efficiency. Additionally, the invasive methods for *in vitro* validation of the bioproducts hampers the translation of basic research to clinical application.

Here, taking advantage of the unique capabilities of MEW over other 3D printing technologies, such as precise control over 3D architecture and superior directional stability of thinner, uniform fibres [52–55], we have designed and fabricated tendon-biomimetic 3D scaffolds that preserved the inherent tensile properties of the murine AT, while emulating their tubular packed bundle characteristic. Furthermore, our computational modeling of the 3D constructs allows for the customization of scaffold design, enabling the creation of patient-specific products tailored to the individual's tendon repair needs. The proposed constitutive law allows for simulating the non-continuous nature of the scaffold using a continuous model, under the assumption that it operates exclusively within the elastic or hyperelastic regime, without accounting for damage. This innovative approach simplifies the modeling process, eliminating the need for complex representations and reducing computational demands [30]. Although further analysis should be performed to verify the validity of the model for different fiber arrangements and printing conditions, this initial approach satisfactorily predicts mechanical behavior close to that obtained experimentally. Moreover, this technique serves as a powerful tool for optimizing scaffold design, ensuring that the methodology can be adjusted to mimic the properties of various tendons, depending on the animal model species and tendon type. Implementing more sophisticated procedures to better determine scaffold porosity will undoubtedly enhance the model's outcomes.

Our tubular 3D scaffolds have been utilized as confinement structures optimized for tenocyte growth and differentiation, intentionally avoiding the direct influence of scaffold pore size and geometry on human tenocyte's features [56–58]. MEW tubular designs have become increasingly popular in various applications [59], including bone tissue engineering and disease modeling [60,61], nerve guides [62], and stents or synthetic vascular grafts [63–66]. Tendon engineering has also benefited from these designs by creating structures that reconstruct injured tendons and improve endogenous tissue healing [45]. The main objective of these previous designs was to provide patterns to enhance cell adhesion and guide tenogenic differentiation [25], by mainly improving cell migration into the scaffold's pore network [67]. Unfortunately, many cells remained at the 3D surface, and although the presence of interconnected thick and thin fibers in longitudinal and transverse positions favored scaffold's mechanical strength, it was in

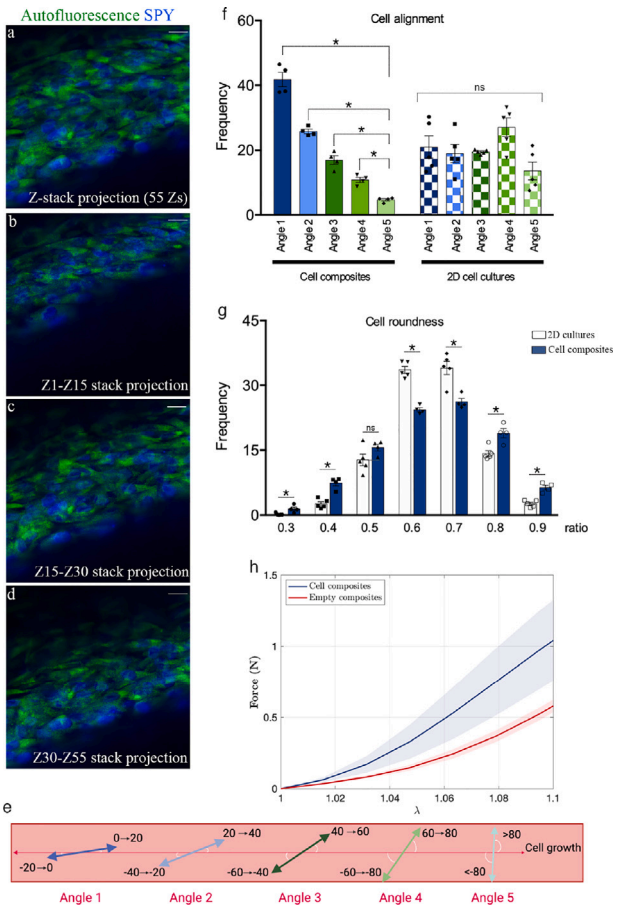

Fig. 8. Representative global z-stack projections (a) and projections from different depths of the same image (b–d) taken form living cell composites after 9 weeks in culture. Nuclei were visualized with SPY. Scale bar: 20 μm. Picture (e) represents the position of cell nuclei within the cell growth axis, showing five varying angles. Graph f represents the quantification of cell alignment in cell composites (n=4) and 2D cell cultures (n=5), showing the frequency of cells in each orientation. Graph g shows the frequency of nuclei roundness in 2D cultures (n=5) and cell composites (n=4), which was measured between 0 and 1. Values being close to 1 represents a rounder cell shape. Graph h shows the stress–strain curves of cell composites (n=4) and cell-free constructs (n=4). Data is expressed as mean±sem and * indicates statistically significant differences between groups, considering $p < 0.05$.

detriment of cell alignment [25,68]. We used two-photon microscopy to track the progression of cell composites over time by leveraging the autofluorescence of both cells and mPCL scaffolds. This method preserves the sample's natural state and enables real-time imaging of living cell composites at depths of up to 500 μm, with 1 μm resolution. Under our conditions, human tenocytes progressively colonized the entire scaffold and became aligned in a controlled orientation along one main longitudinal direction, contributing to nuclei elongation and tensile stress enhancement, suggesting an improved rate of ECM synthesis and deposition. Importantly, these features were found after culturing the cell composites for a 9-week period. Thus, our constructs address the main challenges in producing artificial tendons: guiding stem cell differentiation and preventing the loss of their tenogenic lineage due to time in culture [68].

Material stiffness can influence tenocyte's progression [57,69]. Previous publications suggest that soft substrates can help maintain the tenogenic phenotype of the cells [70], while stiffer matrices might promote cell spreading and proliferation but less differentiation [12,71–73], likely because cells do not tightly attach to soft substrates [74,75]. However, over time, cells loss their fidelity to their growth direction, likely due to the impact of scaffold depth and rigidity on nuclei alignment. Our findings suggest that our tubular scaffold provides a mechanical anisotropy to the tenocytes, enhancing their expansion into the provisional ECM Matrigel. Subsequently, cell-to-cell signaling may amplify nuclei alignment, with cells generating their own ECM and strengthening the microenvironment. This process likely contributes to maintaining cell differentiation over a period of 9 weeks. Thus, we can speculate that tenocytes in our constructs transition from a soft to a stiffer microenvironment in parallel with their cellular progression from expansion to differentiation stages. As a result, our bioproducts consisted of differentiated tenocytes, as evidenced by the expression of scleraxis, tenomodulin, collagen I and decorin proteins, along with increased nuclei alignment and elongation, and enhanced tensile stress—all hallmarks of differentiated tenocytes. Thus, our bioconstructs may prevent the loss of their tenogenic lineage due to time in culture [68], providing sufficient mechanical strength for potential applications in tendon repair. However, this conclusion needs to be tested in future *in vivo* studies. It is important to note that when comparing the force-stretch curves from mechanical tests on scaffolds with and without cells, the latter exhibit lower stiffness than those tested during the initial design phase. This is likely because the scaffolds without cells underwent the same treatments as those with cells, which may have reduced the material properties of PCL while still preserving a stiffer substrate for cell growth and differentiation. PCL is a degradable polymer whose degradation occurs over extended timescales, especially under physiological conditions. This is due to its high crystallinity and hydrophobic nature, which confer excellent mechanical stability and slow degradation rates, making it highly suitable for long-term applications in tissue engineering [31,32,35]. Given the timeframe of our experiments, significant degradation is unlikely to have influenced the mechanical properties of the scaffolds. However, preparation treatments may have influenced the mechanical properties of PCL as reported in the literature for sterilization processes [36].

Tenocytes are more sensitive to mechanical than chemical conditioning regarding cell commitment and the expression of differentiation markers. This may explain the lack of a widely-adopted tenogenic differentiation protocol [51]. Here, we followed a two-step cell culture protocol to emulate the three-step concept for tissue-engineering *in vitro* [76] by first enhancing cell expansion to achieve a maximal number of cells within the entire 3D structure (high serum content), and then inducing and maintaining tenogenic differentiation (low serum content). Cell morphology was influenced by tuning their local mechanical properties through static force applied to the scaffolds, following previous similar strategies [77,78]. Our findings align with recent studies that have demonstrated that as cell density increases, there is a gradual shift from isotropic migration of individual cells to the formation of aligned cell lanes [79], highlighting the importance of cell–cell and cell-ECM interactions in guiding cell destiny. However, the role of serum in driving tenocyte's fate is under continuous debate. For example, tenocytes can be distributed in thick, dense parallel collagen fibres when cultured in high serum media [80], while some other studies have observed the opposite effect, linking serum to tenocyte phenotype drift [28,29,81]. Here, we have shown that tenocytes transitioning from high to low serum media favored the expression of genes and proteins associated with tenocyte-to-tendon conversion. Interestingly, this effect appears to be restricted to younger tenocytes compared to older ones, suggesting a link between tenogenic differentiation and aging, which requires future work.

Study Limitations: We used human-derived cells to better replicate human tendon biology, since the inherent differences between mouse and human cells, especially stem cells and progenitors, may limit the direct relevance of our results to human patients [82]. However, a key limitation of our study is the use of human-derived cells combined with scaffolds designed to mimic the mechanical properties of mouse AT tendons [83] rather than human AT tendons [84]. This decision was made to avoid unnecessary complexity at this stage (e.g.: larger scaffold sizes, advanced mechanical guides, use of bioreactors, etc.) and

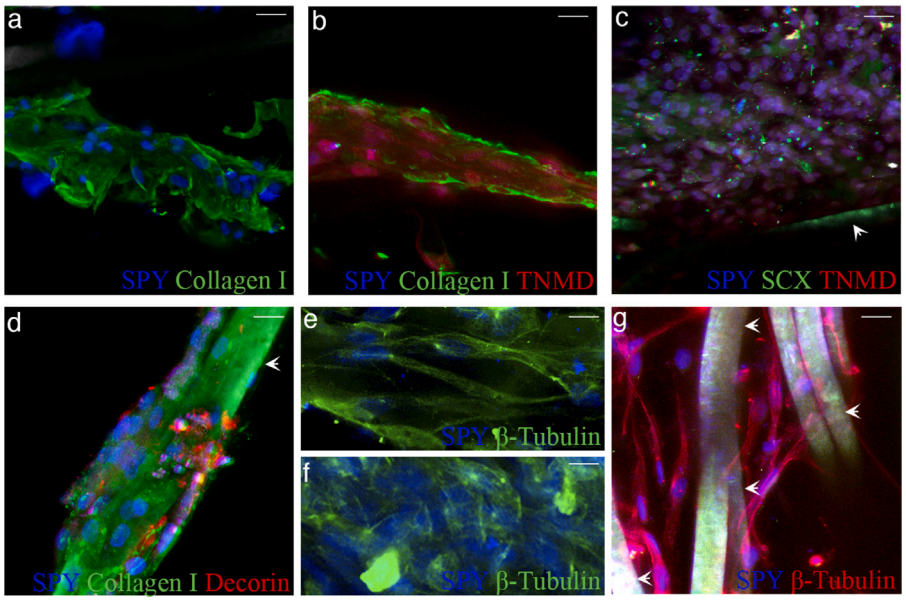

Fig. 9. Representative images of z-stack projections of fixed cell composite sections after 9 weeks in culture immunostained for collagen type I (a), tenomodulin (TNMD, b–c), scleraxis (SCX, c), and/or decorin (d). Images in e–g show z-stack projections from sections immnunostained for β-tubulin. All nuclei were visualized with SPY-DNA. A total of four cell composites were analyzed (n=4). Scale bar: 20 μm.

to focus on cellular interactions and behaviors, such as differentiation and ECM production, while isolating the effect of the scaffold on these cellular responses. The use of mouse tendon mechanics was therefore a simplification, enabling us to investigate the cellular dynamics without introducing confounding variables. We acknowledge that this approach may limit the immediate applicability of our findings to cases of complete human tendon rupture. However, tendon repair often involves partial rather than complete ruptures, which may justify the use of tendon bundles — like those used in our study — over full mechanical constructs, because scaffolds do not necessarily need to fully replicate the mechanical properties of intact human tendons. Additionally, our bio-constructs have the potential to be tested in immunosuppressed mouse models of AT complete rupture, where it is essential for donor and recipient tissues to share similar mechanical properties to reduce graft-host tensile/strain mismatch. In future work, using our computational model, it will be possible to redesign the printing parameters to adjust the biomechanics from the range of mouse AT to the range of human AT. This will allow us to gradually scale up the model, simulate mechanical loading and investigate the effects on human cells in vitro before progressing to more complex in vivo studies. Finally, as the model has been developed based on non-degraded PCL, it presents a limitation due to the observed stiffness loss when preparing the material for culturing. Since this loss can be described as a decrease in the material's constitutive parameters [31], a time-dependent volumetric fraction scaling the strain potential could be fitted to account for it.

5. Conclusion

We have printed MEW-3D tubular scaffolds to mimic the mechanical behavior of mouse AT. By reducing serum content from high to low and applying static mechanical guides, these scaffolds enable the confinement, expansion, and differentiation of human tenocytes without the need for additional biochemical signals. This approach replaces the softer provisional Matrigel ECM with a stiffer, self-generated cellular ECM. Our proposed constitutive law for simulating the scaffold's non-continuous nature using a continuous model simplifies the modeling process, enabling the prediction of mechanical behaviors that closely replicate real-in vivo conditions. This framework will facilitate the scaling up of 3D scaffolds for human tendon rupture applications by transitioning from mouse to human tendon mechanics.

CRediT authorship contribution statement

Jorge Grasa: Writing – review & editing, Writing – original draft, Validation, Software, Methodology, Investigation, Funding acquisition, Formal analysis, Data curation, Conceptualization. **Ainhoa Urbiola:** Investigation, Data curation. **María Flandes-Iparraguirre:** Investigation, Data curation. **Leire Extramiana:** Investigation, Data curation. **Cristina Ederra:** Investigation, Data curation. **Carlos Ortiz-de-Solórzano:** Investigation, Data curation. **Rafael Llombart:** Investigation, Data curation. **Andrés Valentí:** Investigation, Data curation. **Enrique Baquero:** Investigation, Data curation. **Ángel Heras-Sádaba:** Writing – review & editing, Software, Methodology, Investigation, Formal analysis, Data curation, Conceptualization. **Juan Pons-Villanueva:** Writing – review & editing, Validation, Supervision, Methodology, Investigation, Formal analysis, Data curation, Conceptualization. **Begoña Calvo:** Writing – review & editing, Writing – original draft, Visualization, Validation, Supervision, Methodology, Investigation, Funding acquisition, Formal analysis, Data curation, Conceptualization. **Ana Pérez-Ruiz:** Writing – original draft, Visualization, Validation, Supervision, Software, Resources, Project administration, Methodology, Investigation, Funding acquisition, Formal analysis, Data curation, Conceptualization.

Declaration of competing interest

The authors declare the following financial interests/personal relationships which may be considered as potential competing interests: Jorge Grasa reports financial support was provided by Spanish Ministerio de Ciencia, Innovación y Universidades. Ana Perez-Ruiz reports financial support was provided by Spanish Ministerio de Ciencia, Innovación y Universidades. Begona Calvo reports was provided by Department of Industry and Innovation (Government of Aragón). If there are other authors, they declare that they have no known competing financial interests or personal relationships that could have appeared to influence the work reported in this paper.

Acknowledgments

This research was supported by the Spanish Ministerio de Ciencia, Innovación *y* Universidades (Grants PID2020-113822RB-C21, PID2020-113822RB-C22, PID2023-147987OB-C31, and PID2023-147987OB-C33),

the Department of Industry and Innovation of the Government of Aragon (Grant T24-23R, co-financed by Feder), and the Spanish Society of Shoulder and Elbow Surgery (SECHC). Part of the work was performed by the ICTS "NANBIOSIS" specifically by the Tissue and Scaffold Characterization Unit (U13) of the CIBER in Bioengineering, Biomaterials & Nanomedicine (CIBER-BBN at the University of Zaragoza). CIBER actions are financed by the Instituto de Salud Carlos III with assistance from the European Regional Development Fund.

Appendix A. Supplementary data

Supplementary material related to this article can be found online at https://doi.org/10.1016/j.actbio.2025.03.006.

References

[1] Tuomas T. Huttunen, Pekka Kannus, Christer Rolf, Li Felländer-Tsai, Ville M. Mattila, Acute achilles tendon ruptures: Incidence of injury and surgery in Sweden between 2001 and 2012, Am. J. Sport. Med. 42 (10) (2014) 2419–2423.

[2] G. Ho, D. Tantigate, J. Kirschenbaum, J.K. Greisberg, J.T. Vosseller, Increasing age in achilles rupture patients over time, Injury 48 (7) (2017) 1701–1709.

[3] U. Sheth, D. Wasserstein, R. Jenkinson, R. Moineddin, H. Kreder, S.B. Jaglal, The epidemiology and trends in management of acute achilles tendon ruptures in ontario, canada: a population-based study of 27,607 patients, Bone Jt. J. 99-B (2017) 78–86.

[4] Nicholas J. Lemme, Neill Y. Li, Steven F. DeFroda, Justin Kleiner, Brett D. Owens, Epidemiology of achilles tendon ruptures in the United States: Athletic and nonathletic injuries from 2012 to 2016, Orthop. J. Sport. Med. 6 (11) (2018) 2325967118808238.

[5] Oskari Leino, Heli Keskinen, Inari Laaksonen, Keijo Mäkelä, Eliisa Löyttyniemi, Elina Ekman, Incidence and treatment trends of achilles tendon ruptures in Finland: A nationwide study, Orthop. J. Sport. Med. 10 (11) (2022) 23259671221131536.

[6] S. Briggs-Price, J. Mangwani, L. Houchen-Wolloff, G. Modha, E. Fitzpatrick, M. Faizi, et al., Incidence, demographics, characteristics and management of acute achilles tendon rupture: An epidemiological study, PLOS ONE 19 (6) (2024) e0304197.

[7] Simon Svedman, Alejandro Marcano, Paul W. Ackermann, Li Felländer-Tsai, Hans Erik Berg, Acute achilles tendon ruptures between 2002–2021: sustained increased incidence, surgical decline and prolonged delay to surgery—a nationwide study of 53,688 ruptures in Sweden, BMJ Open Sport. Exerc. Med. 10 (2024) e001960.

[8] Arul Subramanian, Thomas F. Schilling, Tendon development and musculoskeletal assembly: emerging roles for the extracellular matrix, Development 142 (24) (2015) 4191–4204.

[9] Christopher Chen, Kenneth J. Hunt, Open reconstructive strategies for chronic achilles tendon ruptures, Foot Ankle Clin. 24 (3) (2019) 425–437.

[10] T. Gregory, U. Hansen, R.J. Emery, B. Augereau, A.A. Amis, Developments in shoulder arthroplasty, Proc. Inst. Mech. Eng. H 221 (1) (2007) 87–96.

[11] Jimin Chen, Jiake Xu, Allan Wang, Minghao Zheng, Scaffolds for tendon and ligament repair: review of the efficacy of commercial products, Expert. Rev Med Devices 6 (1) (2009) 61–73.

[12] Umile Giuseppe Longo, Arianna Carnevale, Ilaria Piergentili, Alessandra Berton, Vincenzo Candela, Emiliano Schena, Vincenzo Denaro, Retear rates after rotator cuff surgery: a systematic review and meta analysis, BMC Musculoskelet. Disord. 22 (1) (2021) 749.

[13] P.V. Komi, S. Fukashiro, M. Järvinen, Biomechanical loading of achilles tendon during normal locomotion, Clin. Sports Med. 11 (3) (1992) 531.

[14] Francesca Veronesi, Veronica Borsari, Deyanira Contartese, Jie Xian, Nicola Baldini, Milena Fini, The clinical strategies for tendon repair with biomaterials: A review on rotator cuff and achilles tendons, J. Biomed. Mater. Res. B Appl. Biomater. 108 (5) (2020) 1826–1843.

[15] Vera Citro, Marta Clerici, Aldo R. Boccaccini, Giovanna Della Porta, Nicola Maffulli, Nicholas R. Forsyth, Tendon tissue engineering: An overview of biologics to promote tendon healing and repair, J. Tissue Eng. 14 (2024) 20417314231196275.

[16] Wei Lee Lim, Ling Ling Liau, Min Hwei Ng, Shiplu Roy Chowdhury, Jia Xian Law, Current progress in tendon and ligament tissue engineering, Tissue Eng. Regen. Med. 16 (6) (2019) 549–571.

[17] Zigang Ge, Fang Yang, James C.H. Goh, Seeram Ramakrishna, Eng Hin Lee, Biomaterials and scaffolds for ligament tissue engineering, J. Biomed. Mater. Res. Part A 77A (3) (2006) 639–652.

[18] Young Jung No, Miguel Castilho, Yogambha Ramaswamy, Hala Zreiqat, Role of biomaterials and controlled architecture on tendon/ligament repair and regeneration, Adv. Mater. 32 (18) (2020) e1904511.

[19] Jingwei Xie, Xiaojian Li, Jennifer Lipner, Christopher N. Manning, Alexander G. Schwartz, Stavros Thomopoulos, Younan Xia, Aligned-to-random nanofiber scaffolds for mimicking the structure of the tendon-to-bone insertion site, Nanoscale 2 (6) (2010) 923–926.

[20] Hannah M. Pauly, Daniel J. Kelly, Ketul C. Popat, Nancy A. Trujillo, Nicolas J. Dunne, Helen O. McCarthy, Tammy L. Haut Donahue, Mechanical properties and cellular response of novel electrospun nanofibers for ligament tissue engineering: Effects of orientation and geometry, J. Mech. Behav. Biomed. Mater. 61 (2016) 258–270.

[21] Chun Liang, Zhe Fan, Zhi Zhang, Peng Wang, Hao Deng, Jing Tao, Electrospinning technology: a promising approach for tendon-bone interface tissue engineering, RSC Adv. 14 (36) (2024) 26077–26090.

[22] Derya C. Surrao, Jonathan C. Fan, Stephen D. Waldman, Brian G. Amsden, A crimp-like microarchitecture improves tissue production in fibrous ligament scaffolds in response to mechanical stimuli, Acta Biomater. 8 (10) (2012) 3704–3713.

[23] Wei Liu, Jennifer Lipner, Christopher H. Moran, Lin Feng, Xiaojian Li, Stavros Thomopoulos, Younan Xia, Generation of electrospun nanofibers with controllable degrees of crimping through a simple, plasticizer-based treatment, Adv. Mater. 27 (16) (2015) 2583–2588.

[24] Steven E. Szczesny, Timothy P. Driscoll, Han-Yu Tseng, Po-Chun Liu, Sung Jin Heo, Robert L. Mauck, Phoebe G. Chao, Crimped nanofibrous biomaterials mimic microstructure and mechanics of native tissue and alter strain transfer to cells, ACS Biomater. Sci. Eng. 3 (11) (2017) 2869–2876.

[25] Gernot Hochleitner, Fei Chen, Carina Blum, Paul D. Dalton, Brian Amsden, Jurgen Groll, Melt electrowriting below the critical translation speed to fabricate crimped elastomer scaffolds with non-linear extension behaviour mimicking that of ligaments and tendons, Acta Biomater. 72 (2018) 110–120.

[26] Go Kaneda, Jonathan L. Chan, Carlos M. Castaneda, Anna Papalamprou, Janna Sheyn, Oleg Shelest, Dawei Huang, Nicholas Kluser, Vincent Yu, Gabriel C. Ignacio, Andrew Gertych, Ryo Yoshida, Michael F. Metzger, William Tawackoli, Gabriel Vernengo, David Sheyn, ipsc-derived tenocytes seeded on microgrooved 3d printed scaffolds for achilles tendon regeneration, J. Orthop. Res.: Off. Publ. Orthop. Res. Soc. 41 (10) (2023) 2205–2220.

[27] K.T. Shalumon, Han-Tsung Liao, Wei-Hao Li, T.G. Darshan, P.A. Mini, Jyh-Ping Chen, Braided suture-reinforced fibrous yarn bundles as a scaffold for tendon tissue engineering in extensor digitorum tendon repair, Chem. Eng. J. 454 (2023) 140366.

[28] L. Yao, C.S. Bestwick, L.A. Bestwick, N. Maffulli, R.M. Aspden, Phenotypic drift in human tenocyte culture, Tissue Eng. 12 (7) (2006) 1843–1849.

[29] Augustus D. Mazzocca, David Chowaniec, Mary Beth McCarthy, Knut Beitzel, Mark P. Cote, William McKinnon, Robert Arciero, In vitro changes in human tenocyte cultures obtained from proximal biceps tendon: multiple passages result in changes in routine cell markers, Knee Surg. Sport. Traumatol. Arthrosc. 20 (9) (2011) 1666–1672.

[30] Cédric P. Laurent, Pierre Latil, Damien Durville, Rachid Rahouadj, Christian Geindreau, Laurent Orgéas, Jean-François Ganghoffer, Mechanical behaviour of a fibrous scaffold for ligament tissue engineering: Finite elements analysis vs. X-ray tomography imaging, J. Mech. Behav. Biomed. Mater. 40 (2014) 222–233.

[31] André C. Vieira, Rui M. Guedes, Volnei Tita, Constitutive modeling of biodegradable polymers: Hydrolytic degradation and time-dependent behavior, Int. J. Solids Struct. 51 (5) (2014) 1164–1174.

[32] Brittany L. Banik, Gregory S. Lewis, Justin L. Brown, Multiscale poly-(ϵ-caprolactone) scaffold mimicking non-linearity in tendon tissue mechanics, Regen. Eng. Transl. Med. 2 (1) (2016) 1–9.

[33] Xiongqi Peng, Zaoyang Guo, Tongliang Du, Woong-Ryeol Yu, A simple anisotropic hyperelastic constitutive model for textile fabrics with application to forming simulation, Compos. Part B: Eng. 52 (2013) 275–281.

[34] Gerhard A. Holzapfel, Thomas C. Gasser, Ray W. Ogden, A new constitutive framework for arterial wall mechanics and a comparative study of material models, J. Elast. Phys. Sci. Solids 61 (1) (2000) 1–48.

[35] Shaun Eshraghi, Suman Das, Mechanical and microstructural properties of polycaprolactone scaffolds with one-dimensional, two-dimensional, and three-dimensional orthogonally oriented porous architectures produced by selective laser sintering, Acta Biomater. 6 (7) (2010) 2467–2476.

[36] Lin Lu, Qingwei Zhang, David M. Wootton, Richard Chiou, Dichen Li, Bingheng Lu, Peter I. Lelkes, Jack Zhou, Mechanical study of polycaprolactone-hydroxyapatite porous scaffolds created by porogen-based solid freeform fabrication method, J. Appl. Biomater. Funct. Mater. 12 (3) (2014) 145–154.

[37] Yiwei Qiu, Xiao Wang, Yaonan Zhang, Andrew J. Carr, Liwei Zhu, Zhidao Xia, Afsie Sabokbar, In vitro two-dimensional and three-dimensional tenocyte culture for tendon tissue engineering, J. Tissue Eng. Regen. Med. 10 (3) (2016) E216–26.

[38] F. Klatte-Schulz, S. Pauly, M. Scheibel, S. Greiner, C. Gerhardt, G. Schmidmaier, B. Wildemann, Influence of age on the cell biological characteristics and the stimulation potential of male human tenocyte-like cells, Eur. Cells Mater. 24 (2012) 74–89.

[39] Antonion Korcari, Samantha J. Przybelski, Anne Gingery, Alayna E. Loiselle, Impact of aging on tendon homeostasis, tendinopathy development, and impaired healing, Connect. Tissue Res. 64 (1) (2022) 1–13.

[40] Chiara Rinoldi, Marco Costantini, Ewa Kijeńska-Gawrońska, Stefano Testa, Ersilia Fornetti, Marcin Heljak, Monika Ćwiklińska, Robert Buda, Jacopo Baldi, Stefano Cannata, Jan Guzowski, Cesare Gargioli, Ali Khademhosseini, Wojciech Swieszkowski, Tendon tissue engineering: Effects of mechanical and biochemical stimulation on stem cell alignment on cell-laden hydrogel yarns, Adv. Heal. Mater. 8 (7) (2019) 1801218.

[41] Kayla Duval, Hannah Grover, Li-Hsin Han, Yongchao Mou, Adrian F. Pegoraro, Jeffery Fredberg, Zi Chen, Modeling physiological events in 2d vs. 3d cell culture, Physiology 32 (4) (2017) 266–277, PMID: 28615311.

[42] Dennis E. Discher, Paul Janmey, Yu li Wang, Tissue cells feel and respond to the stiffness of their substrate, Science 310 (5751) (2005) 1139–1143.

[43] Valentina Angeloni, Nicola Contessi, Cinzia De Marco, Serena Bertoldi, Maria Cristina Tanzi, Maria Grazia Daidone, Silvia Farè, Polyurethane foam scaffold as in vitro model for breast cancer bone metastasis, Acta Biomater. 63 (2017) 306–316.

[44] A.J. Lomas, C.N.M. Ryan, A. Sorushanova, N. Shologu, A.I. Sideri, V. Tsioli, G.C. Fthenakis, A. Tzora, I. Skoufos, L.R. Quinlan, G. O'Laighin, A.M. Mullen, J.L. Kelly, S. Kearns, M. Biggs, A. Pandit, D.I. Zeugolis, The past, present and future in scaffold-based tendon treatments, Adv. Drug Deliv. Rev. 84 (2015) 257–277.

[45] Behzad Shiroud Heidari, Rui Ruan, Ebrahim Vahabli, Peilin Chen, Elena M. De-Juan-Pardo, Minghao Zheng, Barry Doyle, Natural, synthetic and commercially-available biopolymers used to regenerate tendons and ligaments, Bioact. Mater. 19 (2023) 179–197.

[46] Darshan Tagadur Govindaraju, Chih-Hao Chen, K.T. Shalumon, Hao-Hsi Kao, Jyh-Ping Chen, Bioactive nanostructured scaffold-based approach for tendon and ligament tissue engineering, Nanomaterials 13 (12) (2023) 1847.

[47] Chao Ning, Pinxue Li, Cangjian Gao, Liwei Fu, Zhiyao Liao, Guangzhao Tian, Han Yin, Muzhe Li, Xiang Sui, Zhiguo Yuan, Shuyun Liu, Quanyi Guo, Recent advances in tendon tissue engineering strategy, Front. Bioeng. Biotechnol. 11 (2023).

[48] Renqiang Chen, Fanglin Chen, Kenian Chen, Jian Xu, Advances in the application of hydrogel-based scaffolds for tendon repair, Genes Dis. 11 (4) (2024) 101019.

[49] Jingyi Hou, Rui Yang, Ivan Vuong, Fangqi Li, Jiayuan Kong, Hai-Quan Mao, Biomaterials strategies to balance inflammation and tenogenesis for tendon repair, Acta Biomater. 130 (2021) 1–16.

[50] Shunze Cao, Yu Wei, Renheng Bo, Xing Yun, Shiwei Xu, Yanjun Guan, Jianzhong Zhao, Yu Lan, Bin Zhang, Yingjie Xiong, Tianqi Jin, Yuchen Lai, Jiahui Chang, Qing Zhao, Min Wei, Yue Shao, Qi Quan, Yihui Zhang, Inversely engineered biomimetic flexible network scaffolds for soft tissue regeneration, Sci. Adv. 9 (39) (2023).

[51] Ilze Donderwinkel, Rocky S. Tuan, Neil R. Cameron, Jessica E. Frith, Tendon tissue engineering: Current progress towards an optimized tenogenic differentiation protocol for human stem cells, Acta Biomater. 145 (2022) 25–42.

[52] Toby D. Brown, Paul D. Dalton, Dietmar W. Hutmacher, Direct writing by way of melt electrospinning, Adv. Mater. 23 (47) (2011) 5651–5657.

[53] M. Lourdes Muerza-Cascante, David Haylock, Dietmar W. Hutmacher, Paul D. Dalton, Melt electrospinning and its technologization in tissue engineering, Tissue Eng. Part B: Rev. 21 (2) (2015) 187–202.

[54] Paul D. Dalton, Melt electrowriting with additive manufacturing principles, Curr. Opin. Biomed. Eng. 2 (2017) 49–57, Additive Manufacturing.

[55] Paul B. Warren, Zachary G. Davis, Matthew B. Fisher, Parametric control of fiber morphology and tensile mechanics in scaffolds with high aspect ratio geometry produced via melt electrowriting for musculoskeletal soft tissue engineering, J. Mech. Behav. Biomed. Mater. 99 (2019) 153–160.

[56] Ciara M. Murphy, Matthew G. Haugh, Fergal J. O'Brien, The effect of mean pore size on cell attachment, proliferation and migration in collagen-glycosaminoglycan scaffolds for bone tissue engineering, Biomaterials 31 (3) (2010) 461–466.

[57] Timothy M. Maul, Douglas W. Chew, Alejandro Nieponice, David A. Vorp, Mechanical stimuli differentially control stem cell behavior: morphology, proliferation, and differentiation, Biomech. Model. Mechanobiol. 10 (6) (2011) 939–953.

[58] Anne Metje van Genderen, Katja Jansen, Marleen Kristen, Joost van Duijn, Yang Li, Carl C.L. Schuurmans, Jos Malda, Tina Vermonden, Jitske Jansen, Rosalinde Masereeuw, Miguel Castilho, Topographic guidance in melt-electrowritten tubular scaffolds enhances engineered kidney tubule performance, Front. Bioeng. Biotechnol. 8 (2021).

[59] Erin McColl, Jürgen Groll, Tomasz Jungst, Paul D. Dalton, Design and fabrication of melt electrowritten tubes using intuitive software, Mater. Des. 155 (2018) 46–58.

[60] A. Berner, J.D. Boerckel, S. Saifzadeh, R. Steck, J. Ren, C. Vaquette, J. Qiyi Zhang, M. Nerlich, R.E. Guldberg, D.W. Hutmacher, M.A. Woodruff, Biomimetic tubular nanofiber mesh and platelet rich plasma-mediated delivery of bmp-7 for large bone defect regeneration, Cell Tissue Res. 347 (3) (2012) 603–612.

[61] Juan Antonio Romero-Torrecilla, José María Lamo-Espinosa, Purificación Ripalda-Cemborían, Tania López-Martínez, Gloria Abizanda, Luis Riera-Alvarez, Sergio Ruiz de Galarreta-Moriones, Asier López-Barberena, Naiara Rodríguez-Flórez, Reyes Elizalde, Vineetha Jayawarna, José Valdés-Fernández, Miguel Echanove-González de Anleo, Peter Childs, Elena de Juan-Pardo, Manuel Salmeron-Sanchez, Felipe Prósper, Emma Muiños López, Froilán Granero-Moltó, An engineered periosteum for efficient delivery of rhbmp-2 and mesenchymal progenitor cells during bone regeneration, Npj Regen. Med. 8 (1) (2023).

[62] Eugen B. Petcu, Rajiv Midha, Erin McColl, Aurel Popa-Wagner, Traian V. Chirila, Paul D. Dalton, 3D printing strategies for peripheral nerve regeneration, Biofabrication 10 (3) (2018) 032001.

[63] Tomasz Jungst, Iris Pennings, Michael Schmitz, Antoine J.W.P. Rosenberg, Jürgen Groll, Debby Gawlitta, Heterotypic scaffold design orchestrates primary cell organization and phenotypes in cocultured small diameter vascular grafts, Adv. Funct. Mater. 29 (43) (2019) 1905987.

[64] N.T. Saidy, T. Shabab, O. Bas, D.M. Rojas-González, M. Menne, T. Henry, D.W. Hutmacher, P. Mela, E.M. De-Juan-Pardo, Melt electrowriting of complex 3D anatomically relevant scaffolds, Front. Bioeng. Biotechnol. 8 (2020) 793, http://dx.doi.org/10.3389/fbioe.2020.00793, eCollection 2020.

[65] Nele Pien, Dalila Di Francesco, Francesco Copes, Michael Bartolf-Kopp, Victor Chausse, Marguerite Meeremans, Marta Pegueroles, Tomasz Jüngst, Catharina De Schauwer, Francesca Boccafoschi, Peter Dubruel, Sandra Van Vlierberghe, Diego Mantovani, Polymeric reinforcements for cellularized collagen-based vascular wall models: influence of the scaffold architecture on the mechanical and biological properties, Front. Bioeng. Biotechnol. 11 (2023).

[66] Angelica S. Federici, Brooke Tornifoglio, Caitríona Lally, Orquidea Garcia, Daniel J. Kelly, David A. Hoey, Melt electrowritten scaffold architectures to mimic tissue mechanics and guide neo-tissue orientation, J. Mech. Behav. Biomed. Mater. 150 (2024) 106292.

[67] Naomi C. Paxton, Matthew Lanaro, Arixin Bo, Nathan Crooks, Maureen T. Ross, Nicholas Green, Kevin Tetsworth, Mark C. Allenby, YuanTong Gu, Cynthia S. Wong, Sean K. Powell, Maria A. Woodruff, Design tools for patient specific and highly controlled melt electrowritten scaffolds, J. Mech. Behav. Biomed. Mater. 105 (2020) 103695.

[68] Yang Wu, Zuyong Wang, Jerry Ying Hsi Fuh, Yoke San Wong, Wilson Wang, Eng San Thian, Direct e-jet printing of three-dimensional fibrous scaffold for tendon tissue engineering, J. Biomed. Mater. Res. Part B: Appl. Biomater. 105 (3) (2015) 616–627.

[69] Geonhui Lee, Seong-Beom Han, Soo Hyun Kim, Sangmoo Jeong, Dong-Hwee Kim, Stretching of porous poly (l-lactide-co-îÂμ-caprolactone) membranes regulates the differentiation of mesenchymal stem cells, Front. Cell Dev. Biol. 12 (2024).

[70] Andrew English, Ayesha Azeem, Kyriakos Spanoudes, Eleanor Jones, Bhawana Tripathi, Nandita Basu, Karrina McNamara, Syed A.M. Tofail, Niall Rooney, Graham Riley, Alan O'Riordan, Graham Cross, Dietmar Hutmacher, Manus Biggs, Abhay Pandit, Dimitrios I. Zeugolis, Substrate topography: A valuable in vitro tool, but a clinical red herring for in vivo tenogenesis, Acta Biomater. 27 (2015) 3–12.

[71] Kai Ye, Luping Cao, Shiyu Li, Lin Yu, Jiandong Ding, Interplay of matrix stiffness and cell–cell contact in regulating differentiation of stem cells, ACS Appl. Mater. Interfaces 8 (34) (2015) 21903–21913.

[72] Tony Yeung, Penelope C. Georges, Lisa A. Flanagan, Beatrice Marg, Miguelina Ortiz, Makoto Funaki, Nastaran Zahir, Wenyu Ming, Valerie Weaver, Paul A. Janmey, Effects of substrate stiffness on cell morphology, cytoskeletal structure, and adhesion, Cell Motil. Cytoskeleton 60 (1) (2004) 24–34.

[73] Jaime A. Espina, Cristian L. Marchant, Elias H. Barriga, Durotaxis: the mechanical control of directed cell migration, FEBS J. 289 (10) (2021) 2736–2754.

[74] Adam J. Engler, Maureen A. Griffin, Shamik Sen, Carsten G. Bonnemann, H. Lee Sweeney, Dennis E. Discher, Myotubes differentiate optimally on substrates with tissue-like stiffness, J. Cell. Biol. 166 (6) (2004) 877–887.

[75] Wei-hui Guo, Margo T. Frey, Nancy A. Burnham, Yu-li Wang, Substrate rigidity regulates the formation and maintenance of tissues, Biophys. J. 90 (6) (2006) 2213–2220.

[76] Raimund Strehl, Karl Schumacher, Uwe de Vries, Will W. Minuth, Proliferating cells versus differentiated cells in tissue engineering, Tissue Eng. 8 (1) (2002) 37–42.

[77] Nickolay V. Bukoreshtliev, Kristina Haase, Andrew E. Pelling, Mechanical cues in cellular signalling and communication, Cell Tissue Res. 352 (1) (2012) 77–94.

[78] Matthias Ryma, Tina Tylek, Julia Liebscher, Carina Blum, Robin Fernandez, Christoph Böhm, Wolfgang Kastenmüller, Georg Gasteiger, Jürgen Groll, Translation of collagen ultrastructure to biomaterial fabrication for material-independent but highly efficient topographic immunomodulation, Adv. Mater. 33 (33) (2021) 2101228.

[79] Nathaniel P. Skillin, Bruce E. Kirkpatrick, Katie M. Herbert, Benjamin R. Nelson, Grace K. Hach, Kemal Arda Günay, Ryan M. Khan, Frank W. DelRio, Timothy J. White, Kristi S. Anseth, Stiffness anisotropy coordinates supracellular contractility driving long-range myotube-ecm alignment, Sci. Adv. 10 (22) (2024).

[80] Yiwei Qiu, Xiao Wang, Yaonan Zhang, Andrew J. Carr, Liwei Zhu, Zhidao Xia, Afsie Sabokbar, Development of a refined tenocyte expansion culture technique for tendon tissue engineering: In vitrotenocyte expansion for tendon tissue engineering, J. Tissue Eng. Regen. Med. 8 (12) (2012) 955–962.
[81] Marc van Vijven, Stefania L. Wunderli, Keita Ito, Jess G. Snedeker, Jasper Foolen, Serum deprivation limits loss and promotes recovery of tenogenic phenotype in tendon cell culture systems, J. Orthop. Res. 39 (7) (2020) 1561–1571.
[82] Pablo Perel, Ian Roberts, Eugenia Sena, Paul Wheble, Christopher Briscoe, Peter Sandercock, Malcolm Macleod, Luciana E. Mignini, Pradeep Jayaram, Kashif S. Khan, Comparison of treatment effects between animal experiments and clinical trials: systematic review, BMJ (Clin. Res. Ed.) 334 (7586) (2007) 197.
[83] Kiran Pedaprolu, Steven E. Szczesny, Mouse achilles tendons exhibit collagen disorganization but minimal collagen denaturation during cyclic loading to failure, J. Biomech. 151 (2023) 111545.
[84] Thomas A. Wren, S.A. Yerby, Gary S. Beaupré, David R. Carter, Mechanical properties of the human achilles tendon, Clin. Biomech. (Bristol, Avon) 16 (3) (2001) 245–251.